communications physics

Article

https://doi.org/10.1038/s42005-024-01641-6

Chiral limit and origin of topological flat bands in twisted transition metal dichalcogenide homobilayers

Check for updates

Valentin Crépel [1] ✉, Nicolas Regnault[2,3] & Raquel Queiroz[1,3]

The observation of zero field fractional quantum Hall analogs in twisted transition metal dichalcogenides (TMDs) asks for a deeper understanding of what mechanisms lead to topological flat bands in two-dimensional heterostructures, and what makes TMDs an excellent platform for topologically ordered phases, surpassing twisted bilayer graphene. To this aim, we explore the chiral limits of massive Dirac theories applicable to C_3-symmetric moiré materials, and show their relevance for both bilayer graphene and TMD homobilayers. In the latter, the Berry curvature of valence bands leads to relativistic corrections of the moiré potential that promote band flattening, and permit a limit with exactly flat bands with nonzero Chern number. The relativistic corrections enter as a *layer-orbit coupling*, analogous to spin-orbit coupling for relativistic Dirac fermions, which we show is non-negligible on the moiré scale. The Berry curvature of the TMD monolayers therefore plays an essential role in the flattening of moiré Chern bands in these heterostructures.

Extremely narrow bands near magic angle in twisted bilayer graphene (TBG) are natural hosts for strongly correlated phenomena. At the core of the understanding of the TBG phase diagram nevertheless lie single-particle insights[1] that only weakly account for the full interactions of the system. This stems from a hierarchy of energy scales[2] enabling to impose stronger symmetry constraints on theoretical models of TBG at only small costs in their experimental pertinence[3]. The prime example of such physically relevant yet approximate model is the first chiral limit of TBG[4], in which interlayer hopping is neglected where the graphene sheets stand furthest apart in the moiré unit cell. This extreme limit provides Landau-level like[5,6] exact flat bands (EFBs)[7–9] for a twist angle close to the experimental magic value[10]. Relying on this structure, and adapting analytical results on ferromagnetism[11,12] and exact zero modes[13–15] from multi-component Hall systems, it is possible to rationalize the quantum anomalous Hall (QAH) state observed at filling $n = 3$ in presence of aligned hBN[16,17] and the fractional quantum Hall (FQH) states evidenced at low magnetic fields[18].

Twisted transition metal dichalcogenide (TMD) homobilayers have also been identified as prominent platforms for strongly interacting topological phases[19] due to their predicted topological[20] and extremely narrow[21,22] topmost valence bands. Recently, refs. 23,24 have reported clear signatures of strongly correlated physics using compressibility and optical measurements on twisted $MoTe_2$ homobilayers at twist angles $\theta \sim 3.5°$. Independently, these two experiments have detected a robust spin-valley polarized QAH state at unit filling of the moiré unit cell[20,21], which hands down its ferromagnetism below unit filling to realize a half-metal[25] that acts as a precursor to the fractional Chern insulator (FCI), the zero magnetic field analog of the FQHE[26–30], measured at 2/3 filling[23,24].

At the moment, these moiré semiconductors lack the deep analytical structure offered by the approximate models available for TBG, preventing the same level of understanding. This absence of well-controlled theoretical limit for TMDs does not stem from a fundamental opposition with TBG. Indeed, the only difference between moiré TMDs and TBG is a large C_2-symmetry breaking mass term gapping out the Dirac cones, analogous to, but much stronger than, the effect of aligned hBN on TBG[31].

In this article, we comprehensively explore *all* the chiral limits of perturbed Dirac field theories applicable to C_3-symmetric moiré materials. We find that that only two exist, one of which is guaranteed to feature EFBs[4,32,33]. For massless fermions, they reproduce the two chiral limits identified in TBG[3,4]. Extending these limits to massive Dirac theories, we observe that the one possessing topological EFBs perfectly captures the physics of twisted TMD homobilayers. In fact, we argue that, due to larger corrugation effects, TMDs are a better realization of the first chiral limit than TBG itself.

[1]Center for Computational Quantum Physics, Flatiron Institute, New York, NY, USA. [2]Laboratoire de Physique de l'Ecole normale supérieure, ENS, Université PSL, CNRS, Sorbonne Université, Université Paris-Diderot, Sorbonne Paris Cité, Paris, France. [3]Department of Physics, Columbia University, New York, NY, USA. ✉e-mail: vcrepel@flatironinstitute.org

This first massive chiral limit explains the emergence of topological flat bands in TMD homobilayers. Moreover, our approach qualitatively captures the special angles $\theta \sim 3.5°$ where experiments have observed zero-field FCIs[23,24]. The topological character of the flat bands can be understood as a consequence of layer–orbit coupling, the analog of spin–orbit coupling in the standard relativistic Dirac theory. Contrary to the relativistic case however, we show that this term, which to our knowledge does not appear elsewhere, is non-negligible on the moiré scale since the Dirac velocity divided by the moiré period $v/a_m \sim 10$ meV is of similar magnitude as the interlayer hybridization scale.

Index theorems[32–34] guarantee that the flatness of the bands in the chiral limit are, to first order, immune to both gauge and potential disorder akin to the zeroth Landau level of graphene[35]. The existence of this limit, even when fine-tuned, can therefore explain how delicate correlated phases such as FCIs appear in twisted TMDs near their first magic angle despite their disorder and strain.

Results and discussion

EFBs and chiral anomalies

To guide our search for EFBs and magic angles, we build on the physics of TBG, wherein bands closest to charge neutrality perturbatively flatten when the velocity of the Dirac cones vanishes[1], and become fully degenerate under slight modifications of the model that provide a chiral anomaly with non-trivial index[33]. Here, we briefly review these arguments and characterize the most general chiral symmetry applicable to C_3 symmetric moiré materials with Dirac cones.

We consider a two-dimensional heterostructure composed of two layers of massive or massless Dirac materials that hybridize with one another via slowly varying coupling terms on a large moiré scale a_m set by the interlayer lattice mismatch and twist, as described by the generic Hamiltonian

$$h(r) = \begin{bmatrix} \sigma^\mu D_\mu^+ & T^\dagger(r) \\ T(r) & \sigma^\mu D_\mu^- \end{bmatrix}, \tag{1}$$

where $D_\mu^\pm = [\pm\delta\mu, i(v \pm \delta v)\partial_1, i(v \pm \delta v)\partial_2, (m \pm \delta m)]$ includes different velocities $v \pm \delta v$, masses $m \pm \delta m$ and charge neutrality points $\pm\delta\mu$ for the two layers; while the slowly varying hybridization matrix is for the moment left unconstrained and parameterized by $T(r) = (t_j + i\lambda_j)\sigma^j - (t_0 + i\lambda_0)\sigma^0$ with $j = 1, 2, 3$. The σ^μ Pauli matrices represent the spinor structure of the low-energy Dirac fermions, which are distinguished by a layer pseudo-spin τ^μ providing the additional block structure of Eq. (1) with τ^3 defining the layers. Using the gamma matrices $\gamma^0 = \tau^1\sigma^0$, $\gamma^{j=1,2,3} = i\tau^2\sigma^j$, and $\gamma^5 = i\gamma^0\gamma^1\gamma^2\gamma^3$, the action corresponding to h can be compactly recast as (see Supplementary Note 1)

$$\mathcal{S} = \int \mathrm{d}^3x\, \bar\psi\left[i\not{D} + M\right]\psi, \tag{2a}$$

where $x^0 = vt$ represents time, ψ is the fermionic operators with conjugate $\bar\psi = \psi^\dagger\gamma^0$, and we have defined

$$\not{D} = \gamma^a[v\partial_a + it_a\gamma^5 + i\lambda_a(i\gamma^3)] - \delta v\gamma^3\gamma^5\gamma^j\partial_j, \tag{2b}$$

$$M = \delta m + \delta\mu\gamma^0\gamma^3\gamma^5 - m\gamma^3\gamma^5 - t_3\gamma^3 - i\lambda_3\gamma^5, \tag{2c}$$

with $a = 0, 1, 2$ and $j = 1, 2$. Our search for EFBs in this generic model relies on a necessary and a self-consistent condition that we now detail.

First, when the Dirac cones' position is locked by crystalline symmetries, such as C_3 for TBG, perturbative flattening of the bands due to a vanishing Dirac cone velocity serves as a pre-requisite to EFBs. Such vanishing generically occurs upon tuning a single microscopic parameter, e.g., the twist angle, when the co-dimension of the velocity operator is equal to one in the space of possible parameters[36]. The co-dimension of the velocity depends on the symmetries of the Hamiltonian, and in particular cannot equal one in absence of particle-hole (PH) symmetry[36]. Our necessary condition for finding EFBs is therefore that the model Eq. (2a) possess a PH symmetry.

Turning to the self-consistency condition, let us assume the existence of EFBs in our problem. Projected onto these flat bands, the action of Eq. (2a) loses its time dependence and reduces from $(2 + 1)$ to $(2 + 0)$ dimensions, e.g., via $\bar\psi(v\gamma^0\partial_0)\psi = 0$ in the case of degenerate flat bands at zero energy[33]. The previously imposed PH symmetry provides an operator exchanging positive and negative energy states that anti-commutes with the Hamiltonian and plays the role of a chiral symmetry. Since chiral Dirac fermions in even dimensions exhibit a chiral anomaly, the model in Eq. (1) in presence of EFBs must satisfy additional constraints. More precisely, the chiral anomaly forces the effective gauge fields descending from t_a and λ_a, respectively, carried by γ^5 and γ^3 in Eq. (2a), to yield a non-zero integer Atiyah–Singer index[32,37]. This is the self-consistency condition for EFBs, first pioneered in ref. 33, that we will use. This self-consistency condition can be intuitively understood as a Landau-like quantization, since it restrains the flux of chiral gauge fields on elementary real-space patches to integer values; suggesting a deeper connection between such flat bands and generic Landau levels[6].

In fact, the non-trivial Atiyah–Singer index of graphene's Landau levels is the reason why they remain exactly flat even under a non-uniform magnetic field or weak scalar potentials[35,38]. The robustness against varying gauge fields and small perturbations provided by the index theorem is the hidden underlying reason explaining why the phase diagram of TBG is so remarkably reproducible, and why it is so closely connected to the first chiral limit in spite of non-negligible AB-hoppings. Deriving a chiral limit for moiré semiconductors does not only provide a fine tuned EFB model for these materials, but rather argues that such EFBs are resilient to local perturbations through the same anomaly protection present in TBG.

Relying on index theorems[32], PH/chiral symmetries provide self-consistent conditions enabling to localize EFBs in models of coupled Dirac cones[33]. We now exhaustively use this method on our original model Eq. (2a) assuming a moiré pattern with C_3 symmetry.

The chiral limits of C_3 symmetric moiré

We have enumerated all possible PH/chiral symmetries compatible with $v \neq 0$ or $\delta v \neq 0$ that our model may possess *after dimensional reduction*, see Supplementary Note 2 that includes refs. 1,3,4,39,40. Focusing on the most relevant case of C_3-symmetric moiré homobilayers and assuming the lowest harmonics of $T(r)$ are non-zero, we have demonstrated that only two inequivalent PH/chiral symmetries can emerge in our setup (Higher harmonics respecting the C_3-symmetry can be included to the hybridization $T(r)$. They will not change the possible chiral symmetries of the model, but can alter the value of the magic α_c[9].). They correspond to the two inequivalent chiral limits previously identified in TBG[3,4].

The first PH/chiral symmetry, $\gamma^0\gamma^3\gamma^5$, becomes a faithful anti-commuting symmetry of the dimensionally reduced $(2 + 0)$d action provided that it has no mass terms $M = 0$ and that its hybridization assumes the form

$$T^{\mathrm{st}}(r) = t\sum_{n=0}^{2} e^{i(\kappa_n\cdot r)}\begin{bmatrix} 0 & \omega^n \\ \omega^{-n} & 0 \end{bmatrix}, \quad \alpha = \frac{t}{|v\kappa_0|}, \tag{3}$$

with $\omega = \exp(2i\pi/3)$ and κ_n the clockwise $2n\pi/3$ rotation of the moiré Brillouin zone corner κ_0 along $(-\hat y)$, see inset of Fig. 1. This $(2 + 0)$d model exactly reproduces the first chiral limit of TBG[4], whose spectrum only depends on the dimensionless parameter α that is inversely proportional to the twist angle θ. It is known to feature EFBs for equally spaced values of α[7–9]. This result was recovered in ref. 33 by direct evaluation of the Atiyah–Singer index corresponding to Eq. (3), providing integer values n for $\alpha = n\alpha_c$ (see also Supplementary Note 3 that includes refs. 4,33,37). The largest value $\alpha = \alpha_c = 1/\sqrt{3}$ gives an estimate of the first magic angle $\theta_c = 3\sqrt{3}ta/(4\pi v) \simeq 1.1°$[33] close to the experimentally observed value[10].

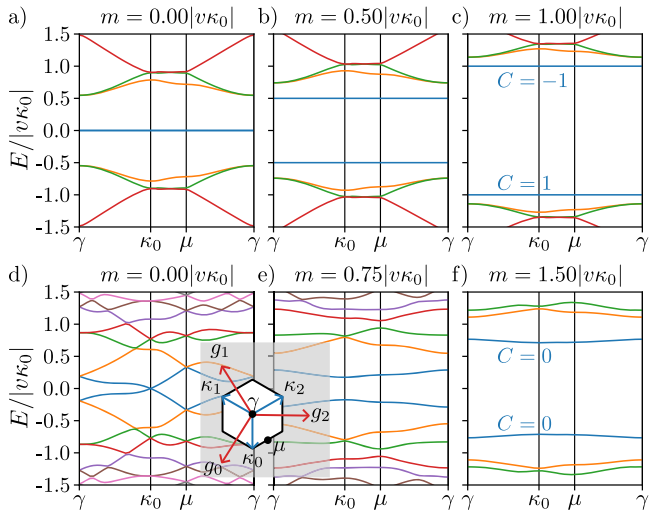

Fig. 1 | Band structure in the two sole massive chiral limits of C_3 symmetric moiré material with Dirac cones in presence of an additional mass m. The first (**a**–**c**) and second (**d**–**f**) chiral limits reproduce those of TBG when $m = 0$ (**a**, **d**) and feature isolated narrow bands for large values of the mass (**c**, **f**). Exact flat bands with opposite Chern numbers appear in the first chiral limit (a-c) for any m due to a chiral anomaly with non-zero Atiyah-Singer index—analogous to the zeroth Landau level of graphene in presence of sublattice potential difference. We used $\alpha = \alpha_c$ in (**a**–**c**, see Eq. (3)), $\alpha = 1.2\alpha_c$ and $r = 0$ in (**d**–**f**, see Eq. (4)), and the inset shows high symmetry points in reciprocal space, with $g_n = \kappa_n - \kappa_{n-1}$.

The second PH/chiral symmetry available, γ^0, requires the $(2+0)$d theory to have $\delta\mu = \delta m = m = 0$ and a specific hybridization matrix

$$T^{\mathrm{nd}}(r) = t\sum\nolimits_{n=0}^{2} e^{i(\kappa_n \cdot r)} \begin{bmatrix} 1+\epsilon & 0 \\ 0 & 1-\epsilon \end{bmatrix}, \tag{4}$$

with ϵ a real parameter. When the system possess an additional C_2 symmetry exchanging the layers' sublattices, $\epsilon = 0$ and the previous form exactly matches the second chiral limit of TBG, describing a perfect metal in which all bands are connected[3,39]. We show in the Supplementary Note 3 that the Atiyah–Singer index vanishes in this second chiral limit, preventing the appearance of EFBs.

Using generic principles and starting from the generic coupled Dirac Hamiltonian Eq. (1), we have identified the two sole chiral limits of C_3-symmetric moiré materials, only one of which provides EFBs due to its non-zero Atiyah-Singer index. The obtained chiral limits reproduce those identified in TBG, which bolsters our approach but also highlights that all EFBs of C_3-symmetric moiré materials feature TBG-like behaviors, in the sense that they derive from the same chiral anomaly.

Consequences for moiré semiconductors

Moiré semiconductors can be described using the $(2+1)$d action in Eq. (2a) with $m \neq 0$. At first sight, this seems to preclude the realization of the chiral limits identified above (Eqs. (3) and (4)) since they both require $m = 0$ in the dimensionally reduced action in $(2+0)$d where the chiral anomaly occurs. Fortunately, these two apparently conflicting theories do not only differ through their mass, but also through their dimensionality. We can thus devise a more general dimensional reduction scheme, compatible with particle-hole symmetry, that transforms the semiconducting $(2+1)$d action with non-zero mass to a massless $(2+0)$d action. This is achieved by projecting the $(2+1)$d action onto flat bands at $\pm m$ using $\bar{\psi} v \gamma^0 \partial_0 \psi = m \psi^\dagger (\gamma^0 \gamma^3 \gamma^5) \psi$, which exactly compensates for the mass terms and yields massless effective $(2+0)$d theories and enables to realize the chiral limits obtained above.

Transposing our previous discussion, we predict that the first massive chiral limit, featuring the hybridization matrix Eq. (3) and a mass m, still has EFBs located at energies $\pm m$. We numerically checked this fact for different m, as shown in Fig. 1a, where we clearly see the originally degenerate flat bands with non-trivial and opposite Chern number splitting to $\pm m$ energies. We have also checked that, as in chiral TBG[5], these flat bands are idea (see Supplementary Note 4 that includes refs. 4–6,41), i.e., equivalent to the physics of a Landau level with non-uniform magnetic field[6]. For small m, this describes the effect of an aligned hBN substrate on chiral TBG[31]. The Chern numbers of the flat bands are inherited from those obtained for TBG in the first chiral limit, and can be understood by analogy with the zeroth Landau levels of graphene, which also split into two groups that can be fully localized on opposite sublattices. Upon adding a sublattice potential difference—equivalent to the mass term in Eq. (1)—these groups with pairwise opposite Chern number acquire finite and opposite energies. While the second chiral limit cannot realize EFBs, we nevertheless highlight that the additional mass term considered here gaps out the perfectly connected bands obtained for $m = 0$, and, for sufficiently large values, produces narrow and isolated trivial bands around charge neutrality (see Fig. 1b).

Compared to TBG, both the first and the second chiral limit yields isolated narrow bands enhancing the interaction effects providing a fertile playground for the emergence of strongly correlated phases. The main difference lies in the topology of these narrow bands: they carry a non-zero Chern number in the first chiral limit and are topologically trivial in the second chiral limit. We finally notice that our method does not work for heterobilayers, for which all four coefficients (v, δv, m, δm) are non-zero in the $(2+1)$d theory and cannot be simultaneously accounted for in the dimensional reduction (see Supplementary Note 2), which suggests that no EFBs exists for semiconducting heterobilayers.

Dirac to Schrödinger and layer–orbit coupling

In presence of large gaps between the conduction and valence bands, an alternative description of the physics of p/n-doped moiré semiconductors should be possible in terms of hole/electron degrees of freedom only. We now derive such description by downfolding our Dirac theory using second order perturbation in the large gap m. We focus on the first massive chiral limit, for it features flat bands and non-trivial topology, and obtain an effective hole-like continuum model describing bands below the band gap. We find a crucial term, neglected in previous works, that differentiates between gapped Dirac physics and simple quadratic bands and provides a simple explanation for the non-trivial topology of the flat bands.

Up to the moiré potential terms, the derivation is identical to the transformation of the massive Dirac equation into the Schrödinger equation with quadratic dispersion. In relativistic settings, small corrections that appear, such as spin–orbit coupling, are inversely proportional to the speed of light. Usually, they can be safely discarded. For moiré materials, they cannot. These corrections are inversely proportional to the Dirac velocity, but $\alpha = \frac{t}{|v\kappa_0|} \sim 1$ implies that they are of the same order as the typical moiré hybridization strength.

Including deviations from the first chiral limit using a hybridization function $T = T^{\mathrm{st}} + \frac{|v\kappa_0|}{2m}\beta T^{\mathrm{nd}}$, where β plays a role analogous to w_0/w_1 in the usual language of TBG[1,39], standard second-order perturbation theory (see Supplementary Note 5 that includes refs. 20,42) gives the effective continuum theory for the valence bands of the moiré semiconductor

$$\begin{aligned} \tilde{h}(r) \;=\; & \tfrac{\hbar^2}{2m^*}\nabla^2\tau^0 - 2V\sum_{n=0,1,2}\cos(g_n\cdot r + \tau^3\psi) \\ & - iW\sum_{n=0,1,2} e^{i\kappa_n\cdot r}\left[1 + i\beta + \tfrac{2\lambda(\kappa_n\times\nabla)}{|\kappa_0|^2}\right]\tau^- + hc, \end{aligned} \tag{5a}$$

with $g_n = \kappa_n - \kappa_{n-1}$ (see inset of Fig. 1), and the global i factor in front of the interlayer-hopping can be gauged away. The coefficients of the downfolded model are inferred from those of the first chiral limit

$$\frac{\hbar^2}{2m^*} = \frac{v^2}{2m},\quad W = \frac{\alpha|\hbar\kappa_0|^2}{2m^*},\quad V = \alpha W,\quad \psi = \frac{2\pi}{3},\quad \lambda = 1. \tag{5b}$$

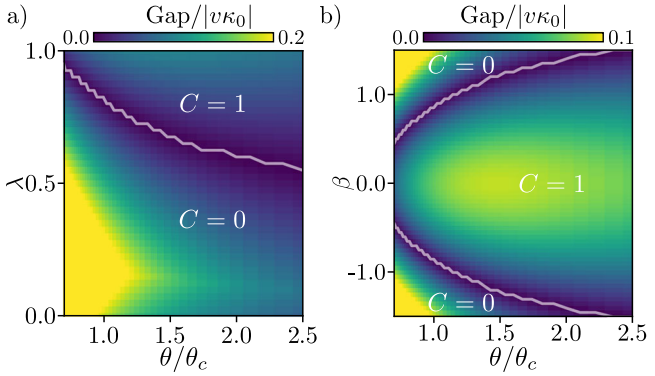

Fig. 2 | Topological phase diagram of chiral moiré semiconductors. a Upon turning off the layer–orbit coupling λ—the analog of spin–orbit coupling in the relativistic Dirac theory, which is *non-negligible* for moiré materials—the topmost valence band from the first chiral limit (Fig. 1a) loses its topological character. All parameters except λ are fixed by Eq. (5a) and $\beta = 0$. **b** Deviations away from the chiral limit (Eq. (5a) with $\lambda = 1$), measured by β, do not spoil the physics of the first massive chiral limit for a wide range of parameters. In both panels, $m = 2|v\kappa_0|$ was used, and $\theta/\theta_c = \alpha_c/\alpha$ since α is inversely proportional to the twist angle.

Thus, up to an overall scaling coefficient, this Hamiltonian only depends on two dimensionless constants (α, β), or only one if we focus on the first chiral limit where $\beta = 0$. The parameters in Eq. (5a) can be combined in magic rule for moiré bilayers with gapped Dirac cones

$$\frac{\hbar^2|\kappa_0|^2}{2m^*}\frac{V}{W^2} = 1 \quad \text{or} \quad E_{\text{kin}}E_{\text{intra}} = E_{\text{inter}}^2, \tag{6}$$

where $E_{\text{kin/inter/intra}}$ stand for the typical kinetic, inter- and intra-layer potential energies on the moiré scale. The rule Eq. (6) determining the magic angle is exact for the massive chiral model with $\beta = 0$. Beyond this model, we speculate that the second formulation in Eq. (6) still provides a good rule of thumb to estimate the twist angle at which correlated physics appears in moiré semiconductors (see Supplementary Note 6 that includes refs. 21,43).

The main difference between Eq. (5a) and previous continuum models for moiré semiconductors[20,21,44] is the advertised layer–orbit coupling λ. This is a non-negligible analog of spin–orbit coupling in relativistic systems. We now stress that this layer–orbit coupling, necessary for a complete down-folding of the Dirac theory, is crucial for the emergence of non-trivial topological properties in moiré semiconductors. For this purpose, we consider Eq. (5a) in the first chiral limit ($\beta = 0$) and consider the effects of turning off λ. In Fig. 2a, we plot the gap between the two topmost valence bands as a function of twist angle, measured by $\alpha_c/\alpha = \theta/\theta_c$, and λ. We observe a topological gap closure as λ goes from its natural value, one, to zero. This proves the crucial role of layer–orbit coupling in Eq. (5a) to capture the topological character of the EFBs obtained in the first massive chiral limit (Fig. 1a).

Including deviations from the first chiral model using $\beta \neq 0$, we can also drive a topological gap closure for sufficiently large values of β (Fig. 2b). The topological character of the topmost valence band obtained in the first chiral limit remains unchanged in a large regime of parameters. For instance, the transition to topologically trivial bands occurs for $\beta \simeq 0.8$ at the magic angle $\alpha = \alpha_c$.

Chirality of TMD homobilayers

We now relate our theory to the physics of twisted K-pocket semiconducting TMD homobilayers, the prime example of exfoliable gapped Dirac cone materials. We argue that, due to corrugation effects, these bilayers lie close to the magic limit than TBG.

In their monolayer form, the considered TMDs display a direct gap between electron and hole pockets at the corner of the Brillouin zone, which can be described as massive Dirac cones of gaps $m \sim 1$–2 eV with

Table 1 | Estimate of the parameters in Eq. (5a) from large-scale ab-initio calculations

Monolayer	m^*	a_0[Å]	Twist [°]	V' [meV]	W' [meV]	β
WSe_2[21]	0.38	3.317	5.08	9	18	0.465
$MoTe_2$[46]	0.62	3.472	4.4	11.2	13.3	0.453
$MoTe_2$[47]	0.62	3.472	3.89	20.8	23.8	0.187

The parameters V' and W' obtained in refs. 21,46,47 for twisted transition metal dichalcogenides homobilayers provide an estimate for β, which plays a role analogous to w_0/w_1 in TBG[1]. It agrees with the result $\beta \simeq 0.54(9)$ obtained by a direct fit of the model Eq. (5a) on the DFT data of ref. 21, described in the Supplementary Note 7.

conduction/valence orbitals mostly of the $d_{z^2}/d_{\pm} = d_{x^2-y^2} \pm id_{xy}$ type near the $\pm K$ corners of the monolayer Brillouin zone. The minimal $k \cdot p$ model describing the twisted TMD homobilayers is thus precisely of the form of Eq. (1). The symmetry of these orbitals determine the form of the interlayer hybridization at high-symmetry stacking points. We focus on R-type (or AA) stacking of the bilayers whose interlayer tunneling matrix T, determined by the symmetry of the bilayer in the lowest-harmonics approximation, is precisely in the form considered above $T = T^{\text{st}} + W\beta T^{\text{nd}}$, ref. 45, with β the ratio between direct interlayer hopping between $d_{\pm}$ orbitals and W.

Whether the first massive chiral model correctly captures the universal physics of these semiconducting TMD homobilayers only depends on the magnitude of β. We now estimate the ratio β using density functional theory results obtained in the literature for specific TMDs (WSe_2 and $MoTe_2$)[21,46,47]. In these references, large-scale ab initio calculations of homobilayers were performed for commensurate twist angle $\theta \sim 4$–$5°$, and the parameters of an effective continuum model describing the bilayer were fitted to the obtained band structure. The resulting continuum model, used to describe $\pm K$-pockets C_3-symmetric moiré semiconducting homobilayers[20,21,44], is related to the one obtained in Eq. (5a) by setting $\lambda = \beta = 0$ and treating (V', W', ψ') as free parameters, where primed variable are used to differentiate from our models.

Neglecting the layer–orbit coupling terms in Eq. (5a) to put both models on the same level, we can identify $W' = W(1 - i\beta)$ up to an irrelevant global phase that can be gauged away. This justifies treating V' and W' as independent parameters of the theory, but also allows to infer the typical values for β from the fitted parameters using $\beta \simeq |W'/\sqrt{V'E_{\text{kin}}} - 1|$ with $E_{\text{kin}} = |\hbar\kappa_0|^2/2m^*$. These estimates are given in Table 1, showing that $\beta \simeq 0.45$ for both $MoTe_2$ and WSe_2 at similar twist angles ~4.5–5° [21,46].

As a final consistency check, we have fitted the full model Eq. (5a), i.e., including layer–orbit coupling, to the band structure of 5.08°-twisted WSe_2 bilayers[21]. To avoid over-fitting, we have first fixed $\lambda = 1$ and used α and β as only free parameters, yielding $\beta = 0.54(9)$ in close agreement with Table 1 (see Supplementary Note 7). To test the relevance of the layer–orbit coupling term, we finally fitted the band structure leaving λ free but keeping α and β fixed to the previously obtained values. This analysis provided the non-negligible best-estimate $\lambda = 0.75(8)$ (see Supplementary Note 7), substantiating the non-negligible role of the layer–orbit coupling highlighted above.

Recall that, in TBG, the dimensionless number playing the role of β is the ratio between AA and AB tunneling amplitudes $w_0/w_1 \simeq 0.6$–0.8, which is larger than our estimate $\beta \simeq 0.5$. Our estimates therefore suggest that twisted TMDs lie closer to the chiral limit than twisted bilayer, providing a simple argument to understand why they may be better hosts for FCIs[23,24]. This difference with TBG is mostly attributable to the stiffer lattice of graphene compared to those of TMDs. Indeed, the stronger lattice relaxation effects in twisted TMDs largely influence the β ratio, because they increase and reduce the inter-layer distance of the homobilayer, respectively, when identical atoms overlap (R_h^h stacking)—decreasing the value of β—and when opposite elements do (R_M^X/R_X^M stacking)—increasing the value of t—where the change in hopping amplitude is exponential in inter-layer distance variations[45].

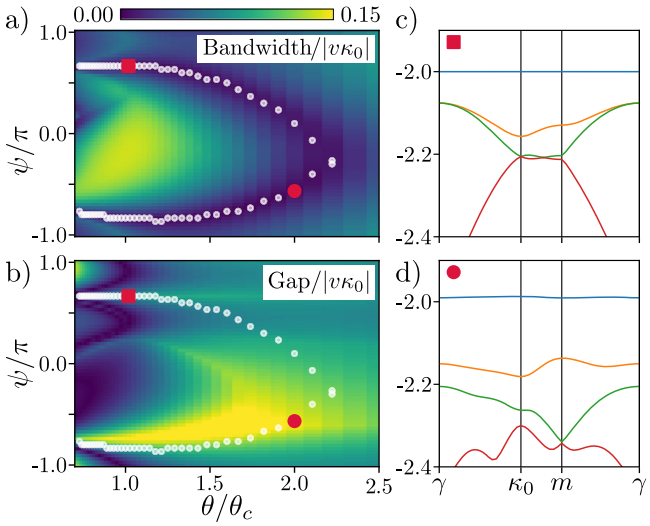

Fig. 3 | Localization of the magic angles for different TMDs. a Bandwidth of the topmost valence band, and **b** direct gap between the two highest valence bands as a function of the twist angle θ and the angle ψ, using $m = 2|v\kappa_0|$. Minima of the bandwidth are highlighted with white dots. We show in (**c**, **d**) the flat band appearing at the points, respectively, identified with a square and a circle in (**a**, **b**). Current literature estimates suggest that (**c**, **d**) are, respectively, relevant for WSe_2[21,43] and $MoTe_2$[20,46]. All parameters are fixed by Eq. (5a) except ψ.

Because such elastic deformations become increasingly dramatic as the twist angle approaches zero[48], the value of β is expected to further decrease in TMD homobilayers at lower twist angles, which can be seen from the much smaller value $\beta \simeq 0.2$ obtained for the fitted parameters of ref. 47 for 3.9°-twisted $MoTe_2$. This argument also reveals that smaller elastic constants are desirable to reach the first massive chiral limit and realize its topological flat band physics in the most pristine fashion. Among all semiconducting TMD monolayers with hexagonal lattice, $MoTe_2$ features the lowest Young modulus[49,50] suggesting its twisted homobilayer form is a slightly better candidate for the emergence of topological correlated phases.

Let us finally comment on the fitted values of ψ' obtained in the literature, which consistently provided $\psi' \simeq -\pi/2$ for $MoTe_2$[20,46] and $\psi' = 2\pi/3$ for WSe_2[21,43]. To grasp the physical consequences of this difference, we investigate the model Eq. (5a) with all parameters fixed in the massive first chiral limit except ψ. Although the PH/chiral symmetry only ensures the presence of EFBs when $\psi = 2\pi/3$, we observe that our downfolded model still displays an extremely narrow topmost valence band in a wide range of angles $-5\pi/6 \le \psi \le 2\pi/3$ (see Fig. 3a), albeit for different values of the twist angle θ. This feature of the model is experimentally desirable for at least two reasons. First, moving along the line of near-zero bandwidth allows to reach parameter regimes for which the gap between the first two valence bands is larger than in the chiral limit (see Fig. 3b). Second, the parameter θ at which the bandwidth almost vanishes are always *larger* than θ_c, leading to larger magic twist angle. The results of Fig. 3 and the fitted values for ψ' given above provide a simple qualitative insight explaining why $MoTe_2$ ($\psi' = -\pi/2$) realizes correlated topological physics for twist angles twice as large as WSe_2 ($\psi' = 2\pi/3$). Our magic rule applied to WSe_2, for which ψ' agrees with Eq. (5a), provides a magic angle $\theta_c \simeq 1.6°$ in agreement with ref. 21. We thus infer $\theta_c \simeq 3.2°$ as magic angle for $MoTe_2$, which is very close to the values 3.4° and 3.7° where FCIs have been recently observed[23,24].

In summary, we have shown that band flattening and exact magic angles in moiré semiconductors can be designed akin to TBG, including the existence of chiral limits. Exact magic angles can be described by chiral anomalies in $(2+0)$d dimensions, which we have fully listed for C_3 symmetric moiré material featuring (gapped or massive) Dirac cones. Only the first chiral limit possess a non-zero Atiyah–Singer index necessary for the emergence of EFB. Our estimates suggests that twisted TMDs lie closer to that limit than TBG with a ratio $\beta \simeq 0.5$ smaller than $w_0/w_1 \simeq 0.6 - 0.8$, providing a natural explanation for the emergence of Landau-level like physics in these systems. Owing to significant corrugation effects, twisted TMDs are arguably a more natural realization of the chiral limit than twisted bilayer graphene itself.

Received: 24 August 2023; Accepted: 22 April 2024;
Published online: 07 May 2024

References

1. Bistritzer, R. & MacDonald, A. H. Moiré bands in twisted double-layer graphene. *Proc. Natl Acad. Sci. USA* **108**, 12233 (2011).
2. Bultinck, N. et al. Ground state and hidden symmetry of magic-angle graphene at even integer filling. *Phys. Rev. X* **10**, 031034 (2020).
3. Song, Z.-D., Lian, B., Regnault, N. & Bernevig, B. A. Twisted bilayer graphene. II. Stable symmetry anomaly. *Phys. Rev. B* **103**, 205412 (2021).
4. Tarnopolsky, G., Kruchkov, A. J. & Vishwanath, A. Origin of magic angles in twisted bilayer graphene. *Phys. Rev. Lett.* **122**, 106405 (2019).
5. Wang, J., Zheng, Y., Millis, A. J. & Cano, J. Chiral approximation to twisted bilayer graphene: exact intravalley inversion symmetry, nodal structure, and implications for higher magic angles. *Physi. Rev. Res.* **3**, 023155 (2021).
6. Estienne, B., Regnault, N. & Crépel, V. Ideal Chern bands as Landau levels in curved space. *Phys. Rev. Res.* **5**, L032048 (2023).
7. Ren, Y., Gao, Q., MacDonald, A. & Niu, Q. WKB estimate of bilayer graphene's magic twist angles. *Phys. Rev. Lett.* **126**, 016404 (2021).
8. Watson, A. B. & Luskin, M. Existence of the first magic angle for the chiral model of bilayer graphene. *J. Math. Phys.* **62**, 091502 (2021).
9. Becker, S., Humbert, T. & Zworski, M. Integrability in the chiral model of magic angles. *Commun. Math. Phys.* **403**, 1153 (2023).
10. Cao, Y. et al. Unconventional superconductivity in magic-angle graphene superlattices. *Nature* **556**, 43 (2018).
11. Sondhi, S. L., Karlhede, A., Kivelson, S. & Rezayi, E. Skyrmions and the crossover from the integer to fractional quantum Hall effect at small Zeeman energies. *Phys. Rev. B* **47**, 16419 (1993).
12. Girvin, S. M. Spin and isospin: exotic order in quantum Hall ferromagnets. *Phys. Today* **53**, 39 (2000).
13. Haldane, F. D. M. Fractional quantization of the Hall effect: a hierarchy of incompressible quantum fluid states. *Phys. Rev. Lett.* **51**, 605 (1983).
14. Trugman, S. & Kivelson, S. Exact results for the fractional quantum Hall effect with general interactions. *Phys. Rev. B* **31**, 5280 (1985).
15. Crépel, V., Regnault, N. & Estienne, B. Matrix product state description and gaplessness of the Haldane-Rezayi state. *Phys. Rev. B* **100**, 125128 (2019).
16. Sharpe, A. L. et al. Emergent ferromagnetism near three-quarters filling in twisted bilayer graphene. *Science* **365**, 605 (2019).
17. Serlin, M. et al. Intrinsic quantized anomalous Hall effect in a moiré heterostructure. *Science* **367**, 900 (2020).
18. Xie, Y. et al. Fractional Chern insulators in magic-angle twisted bilayer graphene. *Nature* **600**, 439 (2021).
19. Mak, K. F. & Shan, J. Semiconductor moiré materials. *Nat. Nanotechnol.* **17**, 686 (2022).
20. Wu, F., Lovorn, T., Tutuc, E., Martin, I. & MacDonald, A. Topological insulators in twisted transition metal dichalcogenide homobilayers. *Phys. Rev. Lett.* **122**, 086402 (2019).
21. Devakul, T., Crépel, V., Zhang, Y. & Fu, L. Magic in twisted transition metal dichalcogenide bilayers. *Nat. Commun.* **12**, 6730 (2021).
22. Crépel, V. & Millis, A. Bridging the small and large in twisted transition metal dicalcogenide homobilayers: a tight binding model capturing orbital interference and topology across a wide range of twist angles. Preprint at https://arxiv.org/abs/2403.15546 (2024).
23. Cai, J. et al. Signatures of fractional quantum anomalous Hall states in twisted $MoTe_2$. *Nature* **622**, 63 (2023).

24. Zeng, Y. et al. Integer and fractional Chern insulators in twisted bilayer $MoTe_2$. Preprint at https://arxiv.org/abs/2305.00973 (2023).
25. Crépel, V. & Fu, L. Anomalous Hall metal and fractional Chern insulator in twisted transition metal dichalcogenides. *Phys. Rev. B* **107**, L201109 (2023).
26. Neupert, T., Santos, L., Chamon, C. & Mudry, C. Fractional quantum Hall states at zero magnetic field. *Phys. Rev. Lett.* **106**, 236804 (2011).
27. Sheng, D., Gu, Z.-C., Sun, K. & Sheng, L. Fractional quantum Hall effect in the absence of Landau levels. *Nat. Commun.* **2**, 389 (2011).
28. Regnault, N. & Bernevig, B. A. Fractional Chern insulator. *Phys. Rev. X* **1**, 021014 (2011).
29. Zhao, S. et al. Fractional quantum Hall effect in valley-layer locked Landau levels in bilayer MoS_2. Preprint at https://arxiv.org/abs/2308.02821 (2023).
30. Crépel, V. & Regnault, N. Attractive Haldane bilayers for trapping non-Abelian anyons. Preprint at https://arxiv.org/abs/2403.05622 (2024).
31. Zhang, Y.-H., Mao, D. & Senthil, T. Twisted bilayer graphene aligned with hexagonal boron nitride: anomalous Hall effect and a lattice model. *Phys. Rev. Res.* **1**, 033126 (2019).
32. Atiyah, M. F. & Singer, I. M. The index of elliptic operators on compact manifolds. *Bull. Am. Math. Soc.* **69**, 422 (1963).
33. Parhizkar, A. & Galitski, V. A generic topological criterion for flat bands in two dimensions. Preprint at https://arxiv.org/abs/2301.00824 (2023).
34. Crépel, V., Ding, P., Verma, N., Regnault, N. & Queiroz, R., Topologically protected flatness in chiral moiré heterostructures. Preprint at https://arxiv.org/abs/2301.00824 (2024).
35. Kailasvuori, J. Pedestrian index theorem à la Aharonov-Casher for bulk threshold modes in corrugated multilayer graphene. *Europhys. Lett.* **87**, 47008 (2009).
36. Sheffer, Y., Queiroz, R. & Stern, A. Symmetries as the guiding principle for flattening bands of Dirac fermions. *Phys. Rev. X* **13**, 021012 (2023).
37. Fujikawa, K. Path-integral measure for gauge-invariant fermion theories. *Phys. Rev. Lett.* **42**, 1195 (1979).
38. Kawarabayashi, T., Hatsugai, Y. & Aoki, H. Quantum Hall plateau transition in graphene with spatially correlated random hopping. *Phys. Rev. Lett.* **103**, 156804 (2009).
39. Bernevig, B. A., Song, Z.-D., Regnault, N. & Lian, B. Twisted bilayer graphene. I. Matrix elements, approximations, perturbation theory, and a k· p two-band model. *Phys. Rev. B* **103**, 205411 (2021).
40. Crépel, V., Dunbrack, A., Guerci, D., Bonini, J. & Cano, J. Chiral model of twisted bilayer graphene realized in a monolayer. *Phys. Rev. B* **108**, 075126 (2023).
41. Crépel, V., Estienne, B., Bernevig, B. A., Lecheminant, P. & Regnault, N. Matrix product state description of Halperin states. *Phys. Rev. B* **97**, 165136 (2018).
42. Crépel, V., Guerci, D., Cano, J., Pixley, J. H. & Millis, A. Topological superconductivity in doped magnetic moiré semiconductors. *Phys. Rev. Lett.* **131**, 056001 (2023).
43. Morales-Durán, N. et al. Pressure-enhanced fractional Chern insulators along a magic line in moiré transition metal dichalcogenides. *Phys. Rev. Res.* **5**, L032022 (2023).
44. Pan, H., Wu, F. & Sarma, S. D. Band topology, Hubbard model, Heisenberg model, and Dzyaloshinskii-Moriya interaction in twisted bilayer wse 2. *Phys. Rev. Res.* **2**, 033087 (2020).
45. Tong, Q., Yu, H., Zhu, Q., Wang, Y., Xu, X. & Yao, W. Topological mosaics in moiré superlattices of van der Waals heterobilayers. *Nat. Phys.* **13**, 356 (2017).
46. Reddy, A. P., Alsallom, F., Zhang, Y., Devakul, T. & Fu, L. Fractional quantum anomalous Hall states in twisted bilayer $MoTe_2$ and WSe_2. *Phys. Rev. B* **108**, 085117 (2023).
47. Wang, C. et al. Fractional Chern insulator in twisted bilayer mote 2. *Phys. Rev. Lett.* **132**, 036501 (2024).
48. Carr, S., Massatt, D., Torrisi, S. B., Cazeaux, P., Luskin, M. & Kaxiras, E. Relaxation and domain formation in incommensurate two-dimensional heterostructures. *Phys. Rev. B* **98**, 224102 (2018).
49. Zeng, F., Zhang, W.-B. & Tang, B.-Y. Electronic structures and elastic properties of monolayer and bilayer transition metal dichalcogenides MX_2 (M= Mo, W; X= O, S, Se, Te): a comparative first-principles study. *Chin. Phys. B* **24**, 097103 (2015).
50. Kastuar, S., Ekuma, C. & Liu, Z.-L. Efficient prediction of temperature-dependent elastic and mechanical properties of 2D materials. *Sci. Rep.* **12**, 3776 (2022).

Acknowledgements

N.R. is grateful to B.A. Bernevig for previous collaboration on related works and enlightening discussions. V.C. thanks L. Fu for insightful discussions on closely connected topics, and X. Petitcol for his hospitality during the critical phase of this work. N.R. acknowledges support from the QuantERA II Programme that has received funding from the European Union's Horizon 2020 research and innovation programme under Grant Agreement No 101017733. N.R. were also supported by the European Research Council (ERC) under the European Union's Horizon 2020 research and innovation programme (grant agreement No. 101020833). Research on topological properties of moiré superlattices is supported as part of Programmable Quantum Materials, an Energy Frontier Research Center funded by the U.S. Department of Energy (DOE), Office of Science, Basic Energy Sciences (BES), under award DE-SC0019443. The Flatiron Institute is a division of the Simons Foundation.

Author contributions

V.C., N.R. and R.Q. conceived of the presented idea. V.C. performed the analytical calculations. All authors discussed the results and contributed to the final manuscript.

Competing interests

The authors declare no competing interests.

Additional information

Supplementary information The online version contains supplementary material available at https://doi.org/10.1038/s42005-024-01641-6.

Correspondence and requests for materials should be addressed to Valentin Crépel.

Peer review information *Communications Physics* thanks Dmitry Efimkin and the other, anonymous, reviewer(s) for their contribution to the peer review of this work